Computational Mechanics 29 (2002) 52–60 © Springer-Verlag 2002
DOI 10.1007/s00466-002-0322-2

On material forces and finite element discretizations

R. Mueller, G. A. Maugin

Abstract The idea of using material forces also termed configurational forces in a computational setting is presented. The theory of material forces is briefly recast in the terms of a non-linear elastic solid. It is shown, how in a computational setting with finite elements (FE) the discrete configurational forces are calculated once the classical field equations are solved. This post-process calculation is performed in a way, which is consistent with the approximation of the classical field equations. Possible physical meanings of this configurational forces are discussed. A purely computational aspect of material forces is pointed out, where material forces act as an indicator to obtain softer discretizations.

Keywords Finite element method, Material force, Eshelbian mechanics

1 Introduction

In an outstanding article Eshelby (1951) introduced the concept of the energy–momentum tensor in continuum mechanics of solids, although at that time Eshelby did not use the term energy–momentum tensor, but preferred the expression Maxwell-tensor of elasticity. The term energy–momentum tensor was introduced later, see Eshelby (1970). In many theories such as the theory of Eshelbian mechanics, the concept of configurational forces or of material forces the energy–momentum tensor appears as a main part. Without claiming completeness we cite the fundamental works of Maugin (1993), Kienzler and Herrmann (2000) and Gurtin (2000). All theories present a general and efficient way to analyze different kinds of material inhomogeneities. It is common to classify the defects or inhomogeneities by their dimensionality. For example zero dimensional (point) defects such as interstitial or foreign atoms in solids can be investigated. The analysis of one dimensional line defects includes for example the treatment of dislocation lines. Two dimensional defects, like interfaces or cracks, and three dimensional inhomogeneities, like inclusions or voids, are other applications of the theory of configurational forces.

The application of material forces addressed in this paper considers discrete material forces introduced by a finite element (FE) discretization. As this is a relatively new application of material forces, which goes back to the work of Braun (1997), we will present some new examples of this application. For more details the reader is also referred to Maugin (2000), Steinmann (2000), Steinmann, Ackermann and Barth (2001) and Mueller, Kolling and Gross (2002). Discrete material forces are derived in a way consistent with the approximation of the field equations. The relevancy of nodal material forces is explained by concerning the change in the total potential of the discrete system with respect to changes in the discretization. A nice feature of discrete material forces is the fact that they can directly be interpreted in terms of the J-integrals in linear elastic fracture mechanics, see Steinmann (2000) and Steinmann, Ackermann and Barth (2001), and driving forces on interfaces, see also Mueller, Kolling and Gross (2002).

2 Theory of material forces

The introduction of configurational forces presented here follows the basic ideas presented in Eshelby (1951) and Eshelby (1970). For brevity of the derivation we consider only elastic materials, but an extension to inelastic settings is possible and discussed in Maugin (1993). For the theoretical part we will restrict attention to quantities that are defined with respect to the reference configuration, because derivations become thus more condensed. However this is not the choice for an efficient numerical implementation, see remark in Sect. 3. For a hyper-elastic material a strain energy function

$$W = \hat{W}(\mathbf{F}, \mathbf{X}) \tag{1}$$

per unit volume of the reference configuration exists. It is assumed that W depends on the deformation gradient $\mathbf{F}$ and explicitly on the position $\mathbf{X}$ (in the reference configuration). The second dependency is introduced to account for inhomogeneous materials. The first Piola–Kirchhoff stress tensor is given by

$$\mathbf{P} = \frac{\partial \hat{W}}{\partial \mathbf{F}} \quad . \tag{2}$$

Received 12 December 2001 / Accepted 18 March 2002

R. Mueller (✉), G. A. Maugin
Laboratoire de Modélisation en Mécanique,
Université Pierre et Marie Curie, Case 162,
4 place Jussieu, 75252 Paris Cedex 05, France

R. Muller was supported by a post-doctoral fellowship within the European "Training and Mobility of Researchers" (TMR) Network on "Phase Transitions in Crystalline Solids". G. A. Maugin benefits from a Max-Planck Award for International Co-operation (2001–2005).

In static equilibrium the Piola–Kirchhoff stress satisfies the equilibrium condition

$$\int_{\partial\mathscr{B}_0} \mathbf{P}\mathbf{N}\,\mathrm{d}A + \int_{\mathscr{B}_0} \mathbf{f}\,\mathrm{d}V = \mathbf{0}\ , \tag{3}$$

which can be expressed in its local form by

$$\mathrm{Div}\ \mathbf{P} + \mathbf{f} = \mathbf{0}\ . \tag{4}$$

The vector $\mathbf{f}$ represents body forces (defined per unit volume of the reference configuration). The material gradient of the strain energy is thus given by

$$\begin{aligned}\mathrm{Grad}\ W &= \mathbf{P} : \mathrm{Grad}\ \mathbf{F} + \left.\frac{\partial \hat{W}}{\partial \mathbf{X}}\right|_{\text{expl.}} \\ &= \mathrm{Div}(\mathbf{F}^{\mathrm{T}}\mathbf{P}) - \mathbf{F}^{\mathrm{T}}\mathrm{Div}\ \mathbf{P} + \left.\frac{\partial \hat{W}}{\partial \mathbf{X}}\right|_{\text{expl.}}\ ,\end{aligned} \tag{5}$$

where in $(5)_1$ the first term in index notation of Cartesian coordinates is given by $P_{ij}F_{ij,K}$. The subscript expl. associated with the second term in (5) denotes the explicit derivative of W with respect to the position $\mathbf{X}$. Rearranging terms together with the mechanical equilibrium condition (4) yields an equation for the material forces in the form

$$\mathrm{Div}\ \boldsymbol{\Sigma} + \mathbf{g} = \mathbf{0}\ , \tag{6}$$

where the configurational stress tensor, the Eshelby stress tensor or the energy-momentum tensor is given by

$$\boldsymbol{\Sigma} = W\mathbf{1} - \mathbf{F}^{\mathrm{T}}\mathbf{P} \tag{7}$$

and the configurational force

$$\mathbf{g} = -\mathbf{F}^{\mathrm{T}}\mathbf{f} - \left.\frac{\partial \hat{W}}{\partial \mathbf{X}}\right|_{\text{expl.}} \tag{8}$$

is introduced to obtain a formula that resembles the structure of equation (4). Introducing the symmetric second Piola–Kirchhoff stress tensor $\mathbf{S}$, and the symmetric right Cauchy–Green tensor $\mathbf{C}$, defined by

$$\mathbf{S} = \mathbf{F}^{-1}\mathbf{P} \quad \text{and} \quad \mathbf{C} = \mathbf{F}^{\mathrm{T}}\mathbf{F} \tag{9}$$

respectively, (7) can be written as

$$\boldsymbol{\Sigma} = \mathbf{W}\mathbf{1} - \mathbf{C}\mathbf{S}, \quad \text{thus} \quad \boldsymbol{\Sigma}\mathbf{C} = \mathbf{C}\boldsymbol{\Sigma}^{\mathrm{T}}\ . \tag{10}$$

The last expression can be thought of as symmetry of the energy-momentum tensor Σ with respect to right Cauchy-Green tensor $\mathbf{C}$. From (6) an important observation can be made: If the body is homogeneous and no body forces are applied, the divergence of the energy–momentum tensor vanishes, i.e.

$$\mathrm{Div}\ \boldsymbol{\Sigma} = \mathbf{0}\ . \tag{11}$$

Thus within the body the energy–momentum tensor satisfies a strict conservation law. On a discussion of conservation laws, see for example Kienzler and Herrman (2000). This is an important property, that will be used in the subsequent applications.

For the computational setting a FE formulation in the actual configuration is chosen, as this formulation is more efficient – for a detailed discussion the reader is referred to Wriggers (2001). The formulation in the actual configuration uses the Cauchy stresses, which are related to the first and second Piola–Kirchhoff stresses through

$$\boldsymbol{\sigma} = \frac{1}{J}\mathbf{P}\mathbf{F}^{\mathrm{T}} \quad \text{or} \quad \boldsymbol{\sigma} = \frac{1}{J}\mathbf{F}\mathbf{S}\mathbf{F}^{\mathrm{T}} \quad \text{with} \quad J = \det\mathbf{F}\ . \tag{12}$$

With this relation the energy–momentum tensor can alternatively be expressed using Cauchy stresses by

$$\boldsymbol{\Sigma} = W\mathbf{1} - J\mathbf{F}^{\mathrm{T}}\boldsymbol{\sigma}\mathbf{F}^{-\mathrm{T}}\ . \tag{13}$$

3 Finite elements

As has been mentioned in the theory section the (material) divergence of the energy–momentum is zero for a homogeneous body without body forces. This property is used to check discrete solutions obtained by FE. As FE solutions are just approximations, the non-vanishing of the divergence of the energy-momentum tensor is an error indicator. Starting from a weak formulation of (6) with a test function $\boldsymbol{\eta}$,

$$\int_{\mathscr{B}_0} (\mathrm{Div}\ \boldsymbol{\Sigma} + \mathbf{g}) \cdot \boldsymbol{\eta}\ \mathrm{d}V = 0 \tag{14}$$

integration by parts (used to transfer derivatives to the test function) yields:

$$\begin{aligned}&\int_{\partial\mathscr{B}_0} (\boldsymbol{\Sigma}\mathbf{N}) \cdot \boldsymbol{\eta}\ \mathrm{d}A - \int_{\mathscr{B}_0} \boldsymbol{\Sigma} : \mathrm{Grad}\ \boldsymbol{\eta}\ \mathrm{d}V \\ &\quad + \int_{\mathscr{B}_0} \mathbf{g} \cdot \boldsymbol{\eta}\ \mathrm{d}V = 0\ .\end{aligned} \tag{15}$$

Assuming that the test function $\boldsymbol{\eta}$ vanishes on the boundary $\partial\mathscr{B}_0$, the first integral in (15) is zero. This assumption represents a stationary boundary – a stationary boundary is a boundary that does not change its (material/referential) position $\mathbf{X}$.

In the following the case of 3D problems will be considered. For plane strain problems, as will be dealt with in the example section, the reduction is straight forward and is not explained in detail here. The classical mechanical quantities are treated in the standard way using an iso-parametric concept for interpolating the displacement field. After solving the equilibrium equations the discrete FE approximation provides the displacement field $\mathbf{u}$ at every point. For the configurational force balance the same concept is utilized. The test function in (15) is approximated in every element $\mathscr{B}_e$ by node values $\boldsymbol{\eta}^I$ and shape functions N^I:

$$\underline{\boldsymbol{\eta}} = \sum_I N^I \underline{\boldsymbol{\eta}}^I, \quad \text{where } \underline{\boldsymbol{\eta}} = \begin{Bmatrix}\eta_1\\ \eta_2\\ \eta_3\end{Bmatrix} \quad \text{and } \underline{\boldsymbol{\eta}}^I = \begin{Bmatrix}\eta_1^I\\ \eta_2^I\\ \eta_3^I\end{Bmatrix}\ . \tag{16}$$

Using a matrix notation for the gradient of the test function and the energy–momentum tensor in the following way

$$\underline{\text{Grad}\ \boldsymbol{\eta}} = \begin{Bmatrix} \eta_{1,1} \\ \eta_{2,2} \\ \eta_{3,3} \\ \eta_{1,2} \\ \eta_{2,1} \\ \eta_{2,3} \\ \eta_{3,2} \\ \eta_{3,1} \\ \eta_{1,3} \end{Bmatrix} = \sum_I \underline{\mathbf{D}}^I \underline{\boldsymbol{\eta}}^I,$$

$$\text{where} \quad \underline{\mathbf{D}}^I = \begin{bmatrix} N^I_{,X_1} & 0 & 0 \\ 0 & N^I_{,X_2} & 0 \\ 0 & 0 & N^I_{,X_3} \\ N^I_{,X_2} & 0 & 0 \\ 0 & N^I_{,X_1} & 0 \\ 0 & N^I_{,X_3} & 0 \\ 0 & 0 & N^I_{,X_2} \\ 0 & 0 & N^I_{,X_1} \\ N^I_{,X_3} & 0 & 0 \end{bmatrix},$$

$$\underline{\boldsymbol{\Sigma}} = \begin{Bmatrix} \Sigma_{11} \\ \Sigma_{22} \\ \Sigma_{33} \\ \Sigma_{12} \\ \Sigma_{21} \\ \Sigma_{23} \\ \Sigma_{32} \\ \Sigma_{31} \\ \Sigma_{13} \end{Bmatrix} \quad \text{and} \quad \underline{\mathbf{g}} = \begin{Bmatrix} g_1 \\ g_2 \\ g_3 \end{Bmatrix} \tag{17}$$

yields

$$-\int_{\mathscr{B}_e} (\underline{\text{Grad}\ \boldsymbol{\eta}})^{\mathrm{T}} \cdot \underline{\boldsymbol{\Sigma}}\, \mathrm{d}V + \int_{\mathscr{B}_e} \underline{\boldsymbol{\eta}}^{\mathrm{T}} \cdot \underline{\mathbf{g}}\, \mathrm{d}V = 0 \ . \tag{18}$$

Note that the standard Voigt-notation for symmetric tensors can not be used, as the energy-momentum tensor is not in general symmetric, see remarks in previous section. In fact from (10) it is obvious that Σ is in general only symmetric if an isotropic material is considered (i.e. $\mathbf{C}$ and $\mathbf{S}$ have identical eigenvectors). Inserting the above approximations the relation

$$\sum_I \underline{\boldsymbol{\eta}}^{I^{\mathrm{T}}} \cdot \left[-\int_{\mathscr{B}_e} \underline{\mathbf{D}}^{I^{\mathrm{T}}} \cdot \underline{\boldsymbol{\Sigma}}\, \mathrm{d}V + \int_{\mathscr{B}_e} N^I \underline{\mathbf{g}}\, \mathrm{d}V \right] = 0 \tag{19}$$

is obtained for the weak form (15). As the equation must be satisfied for arbitrary node values $\boldsymbol{\eta}^I$, the term in square brackets must vanish. This introduces discrete configurational forces in a natural way as

$$\underline{\mathbf{G}}^I_e = \begin{Bmatrix} G^I_{e1} \\ G^I_{e2} \\ G^I_{e3} \end{Bmatrix} = \int_{\mathscr{B}_e} N^I \underline{\mathbf{g}}^I\, \mathrm{d}V = \int_{\mathscr{B}_e} \underline{\mathbf{D}}^{I^{\mathrm{T}}} \cdot \underline{\boldsymbol{\Sigma}}\, \mathrm{d}V$$
$$= \int_{\mathscr{B}_e} \begin{Bmatrix} N^I_{,X_1}\Sigma_{11} + N^I_{,X_2}\Sigma_{12} + N^I_{,X_3}\Sigma_{13} \\ N^I_{,X_1}\Sigma_{21} + N^I_{,X_2}\Sigma_{22} + N^I_{,X_3}\Sigma_{23} \\ N^I_{,X_1}\Sigma_{31} + N^I_{,X_2}\Sigma_{32} + N^I_{,X_3}\Sigma_{33} \end{Bmatrix} \mathrm{d}V \ . \tag{20}$$

The configurational forces $\mathbf{G}^I_e$ of all n_e elements adjacent to node K then need to be assembled to give the total configurational force

$$\underline{\mathbf{G}}^K = \bigcup_{e=1}^{n_e} \underline{\mathbf{G}}^I_e \ . \tag{21}$$

We emphasize again that this does not pose a new boundary value problem, as the nodal values $\mathbf{G}^K$ are obtained purely from quantities that are already known (strain energy, stresses and deformation measures) from the solution of the displacement field. The calculation of the discrete configurational forces is thus just a post-processing procedure.

4 Examples

4.1 Material parameters

Throughout this paper we will consider a non-linear elastic material, with an isotropic strain energy W of the Neo-Hookean type given by

$$W(I_C, J) = \frac{\lambda}{2}\left(\frac{J^2-1}{2} - \ln J\right) + \frac{\mu}{2}(I_C - 3 - 2\ln J) \ , \tag{22}$$

where $I_C = \mathrm{tr}\ \mathbf{C}$ is the first invariant of the right Cauchy–Green tensor $\mathbf{C}$, see Wriggers (2001). The material parameters λ and μ represent the Lamé constants in the small strain limit. From the strain energy the second Piola–Kirchhoff stress can be computed by

$$\mathbf{S} = 2\frac{\partial W}{\partial \mathbf{C}} = \mu\big(\mathbf{1} - \mathbf{C}^{-1}\big) + \frac{\lambda}{2}\big(J^2 - 1\big)\mathbf{C}^{-1} \ . \tag{23}$$

Using (12) the Cauchy stresses, which are used in the solution of the standard field equations are given by

$$\boldsymbol{\sigma} = \frac{\mu}{J}(\mathbf{B} - \mathbf{1}) + \frac{\lambda}{2J}\big(J^2 - 1\big)\mathbf{1} \ , \tag{24}$$

where $\mathbf{B} = \mathbf{F}\mathbf{F}^{\mathrm{T}}$ is the left Cauchy–Green tensor. For the computation of the tangential stiffness matrix the material tangent is needed. For the given material the Cartesian components of the material tangent in the reference configuration are given by

$$\mathbb{C}_{IJKL} = 2\frac{\partial S_{IJ}}{\partial C_{KL}} = \lambda J^2 (C^{-1})_{IJ}(C^{-1})_{KL} + \frac{2\mu - \lambda(J^2-1)}{2}\Big((C^{-1})_{IK}(C^{-1})_{LJ} + (C^{-1})_{IL}(C^{-1})_{JK}\Big) \tag{25}$$

and in the actual configuration by

$$\mathbb{c}_{ijkl} = \lambda J \delta_{ij}\delta_{kl} + \frac{2\mu - \lambda(J^2-1)}{2J}\left(\delta_{ik}\delta_{lj} + \delta_{il}\delta_{jk}\right) \ . \tag{26}$$

From the above equation the computational advantage of a formulation in the actual configuration can be seen. In the actual configuration the material tangent is not fully populated. In addition the B-matrix is not fully populated (see standard literature on non-linear FE for this, e.g. Wriggers (2001)), which together allows for more efficient implementation as less multiplications are needed to form the element stiffness matrix.

4.2
Homogeneous block

The first example consists of a block of homogeneous material ($\lambda = 1000, \mu = 400$), which is loaded by a displacement w on its top side, see Fig. 1a for a sketch of the problem. For this 2D problem a state of plane strain is assumed. The discrete material forces at the node points are depicted in Fig. 1b. It is observed that large material forces occur at the boundary. From the theoretical derivation of Sect. 2 no material forces should appear in the interior, see Eq. (11), as the block is homogeneous. However the FE approximation introduces some spurious material node forces that originate from the fact that the approximation is not smooth with respect to strains (and stresses). Therefore in the interior the numerical value of the nodal material forces does not vanish. As material points on the boundary are not allowed to change their position in the reference configuration, material forces appear as reaction forces to this constraint.

An obvious question is to ask if there exists an internal arrangement of nodes for which the material forces vanish, as they should from a theoretical point of view. As this question is a finite dimensional optimization problem (which may not be convex), we take as a first illustrative question the following: Is it possible to find a X_2-position for the marked point in Fig. 2a and its symmetrical partner, so that the configurational forces on this points vanish? The considered mesh changes are also sketched in Fig. 2a. The dependence of the material force G_2 is shown in Fig. 2b. For this node the specific position that satisfies the demand is at $X_2/a \approx 0.3$. In a further example all interior nodes are allowed to move. The position of the interior nodes is updated by the following rule

$$\mathbf{X}^K \rightarrow \mathbf{X}^K - c\mathbf{G}^K \ , \tag{27}$$

where K represents all interior nodes. It must be mentioned that the constant c is to be chosen sufficiently small to achieve convergence (to avoid "unhealthy" mesh distortions). The result of this updating technique is presented in Fig. 3a. It is interesting to note that the mesh modification softens the system, as can be seen from Fig. 3b. There the force F resulting from the displacement of the top surface is plotted during the update process. However, the change in reaction force is relatively small, as one would deduce from the relative moderate mesh modifications.

4.3
Cantilever beam with square hole

This example is a theoretical examination of the relation between a defect, in this case a square hole, and the associated material forces. A rectangular block that is clamped at one side and loaded by a vertical displacement on the other side is considered, see Fig. 4a. This loading situation resembles a cantilever beam. In Fig. 4b the distribution of the σ_{11}-stress component is shown together with the starting position of the hole. The stress distribution is similar to the distribution of the bending stress known from technical beam theory. As the hole is placed in the vertical center near the neutral phase, it only slightly disturbs the stress distribution. The resulting material force on the hole is evaluated by

$$\mathbf{G}_{\text{hole}} = \sum_{K=1}^{N_{\text{hole}}} \mathbf{G}^K \ , \tag{28}$$

where all N_{hole} material forces of nodes, which are located on the boundary of the hole are summed up. A "kinetic relation" for the motion of the hole is proposed in the following way

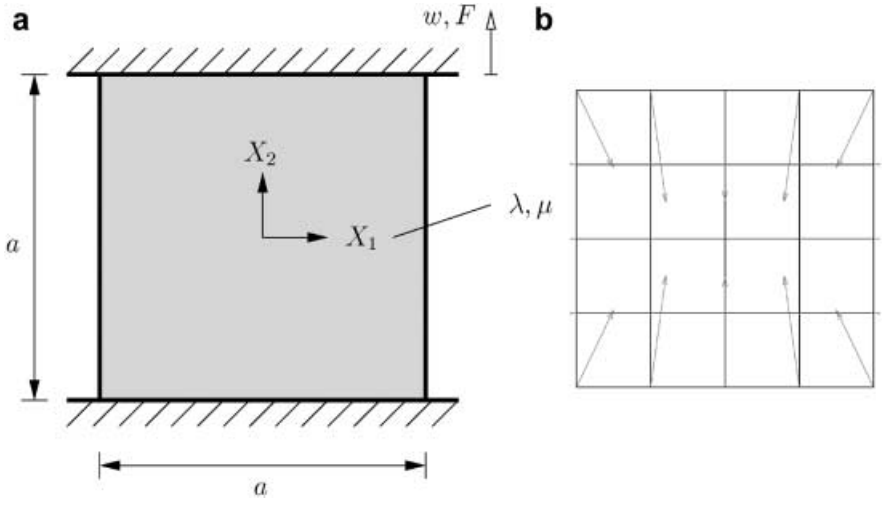

Fig. 1. Homogeneous block: **a** sketch of problem, **b** discrete material forces

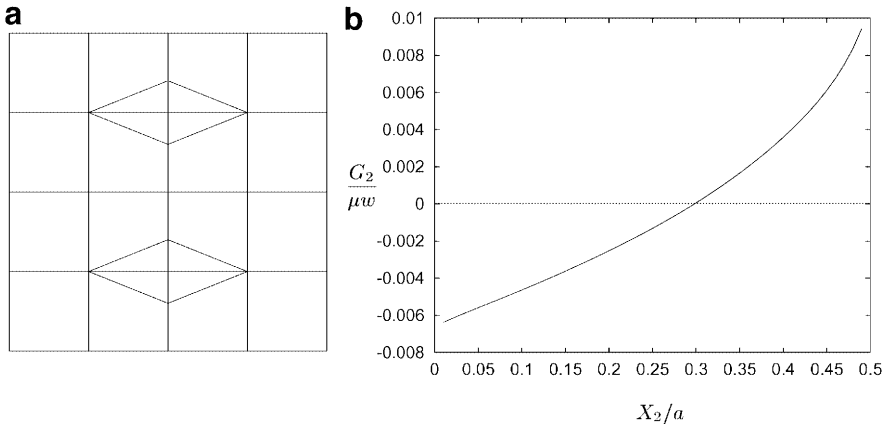

Fig. 2. Homogeneous block: **a** changes in the mesh, **b** material force

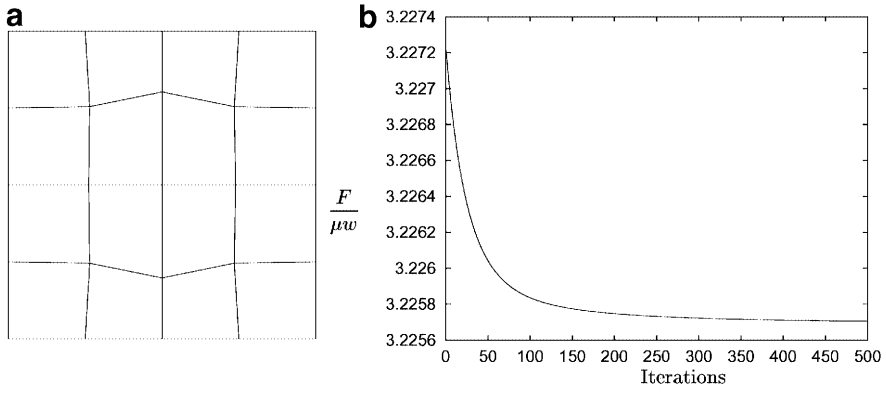

Fig. 3. Mesh modification: **a** final mesh, **b** change in reaction force F

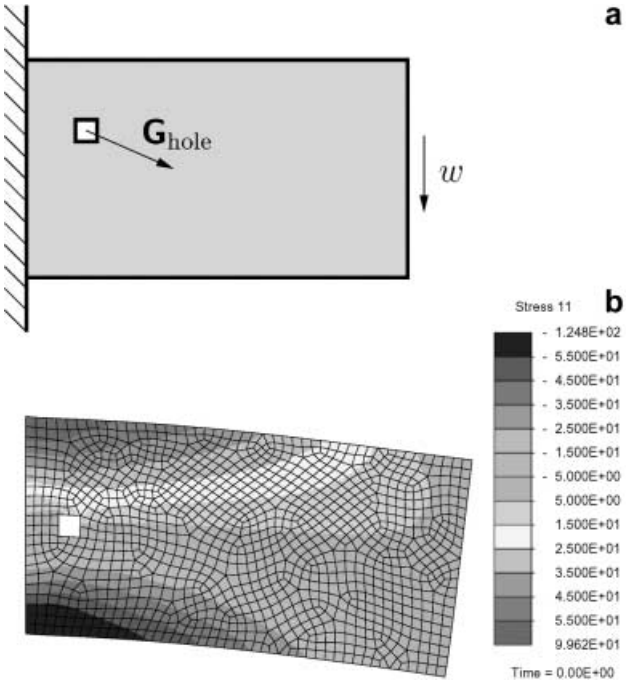

Fig. 4. Cantilever beam: **a** boundary conditions, **b** distribution of σ_{11}

$$\mathbf{X}_{\text{hole}}^{\text{new}} \rightarrow \mathbf{X}_{\text{hole}}^{\text{old}} - c\mathbf{G}_{\text{hole}} \ , \tag{29}$$

where we choose c such that

$$|\mathbf{X}_{\text{hole}}^{\text{new}} \rightarrow \mathbf{X}_{\text{hole}}^{\text{old}}| = b = \text{const} \ . \tag{30}$$

This can be interpreted as a motion of the hole with "constant velocity". A general remark is necessary at this point. As the physical process which allows a hole to move through a solid body has not been specified, this example is of purely academic/theoretical nature. If the hole is interpreted as an "over" simplified model of a vacancy or a void, one might think of diffusion or corrosion processes that allow the hole to move through the body. Figure 5 shows the movement of the hole through the body. It can be seen that the hole as an inhomogeneity is driven out of the body by the material forces. After each position change of the hole a new mesh is generated to avoid a deterioration of the discretization. In order to illustrate the path of the hole the trajectory is also given in the plots of Fig. 5. After 12 iterations the calculation is stopped as the hole reaches the boundary and the automatic mesh generation breaks down. If one tries different starting points, the material forces will always try to drive the inhomogeneity out of the body, i.e. to render the total body more "homogeneous". For example a slightly shifted down starting position, will lead to a trajectory where the hole leaves the block on the lower boundary.

4.4 Simulation of crack propagation using material forces

This 2D simulation resembles a compact-tension (CT) specimen which is loaded by a dead displacement w, for a sketch of the situation see Fig. 6a. A state of plane strain is

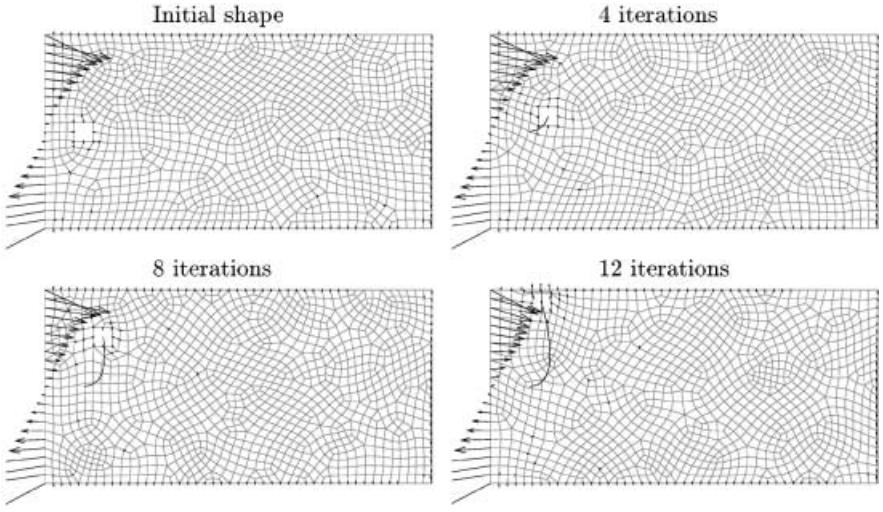

Fig. 5. Cantilever beam: material forces and trajectory of hole

assumed. A circular hole is introduced in the specimen to study the interaction of material forces at the crack-tip with the material forces caused by the hole. The initial distribution of material forces **G** is plotted in Fig. 6b. At the points where the displacement boundary conditions are applied, and at the crack-tip large material forces are observed. In the close vicinity of the crack tip material forces occur due to the inaccurate approximation of the large gradients in the crack tip region. From a theoretical point of view these forces should vanish, compare Eq. (11). In the situation in Fig. 6b the hole is placed relatively far from the crack tip. Crack propagation is assumed to take place according to the simple rule

$$\mathbf{X}^{\text{new}}_{\text{crack-tip}} \rightarrow \mathbf{X}^{\text{old}}_{\text{crack-tip}} - c\mathbf{G}_{\text{crack-tip}} \quad . \tag{31}$$

The proportionality constant c has to be chosen in an appropiate way, i.e. the crack propagation has to be sufficiently small and at the same time large enough to ensure a proper mesh generation for the new geometry. It is mentioned, that no threshold for crack initiation is introduced, as this study is supposed to have only qualitative character. A crack initiation value can be found for example by considering a Griffith energy criterion, for details see e.g. Gross (1996). It is also mentioned, that the crack propagation is determined in size and direction by the material forces. Another possibility to determine the propagation direction is the criterion of maximal circumferential stress as proposed by Erdogan and Sih, see also Gross (1996).

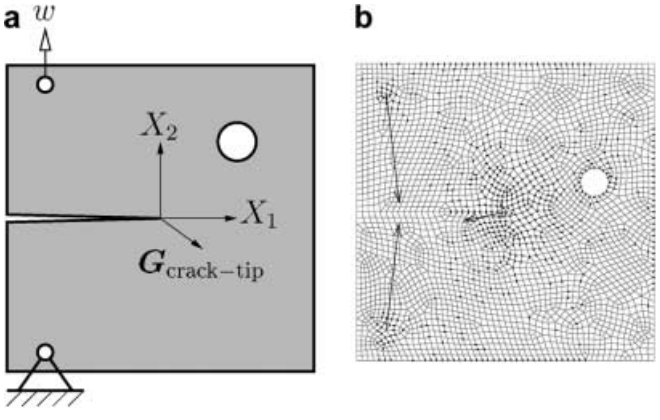

Fig. 6. Crack propagation: **a** problem situation, **b** material forces

Being aware of all these simplifications two different initial situations are analyzed. In the first simulation (Fig. 7) the hole is placed relatively far away from the crack, so that during crack propagation the crack reaches the hole by slightly changing its direction. The simulation is stopped just before the crack reaches the hole, because in this situation the automatic mesh generation fails. In the second situation the hole is moved horizontally closer to the crack tip, see Fig. 8. Now the crack tip does not change direction rapidly enough to reach the hole and passes the hole. However the crack path is significantly perturbed by the hole.

4.5 Block under constant pressure

The first 3D example is a cubic block with edge length a, which is loaded on one quarter of its top by a pressure dead load p_0, for a sketch see Fig. 9a. The stress distribution in the loading direction is given in Fig. 9b. The contour lines of the stress are not very smooth and experience kinks at element edges. Using the updating rule (27) the positions of the interior nodes is modified. The modification process is depicted in Fig. 10, where a central cut of the mesh is given. The nodes are attracted by the point where the load is applied, as there are more pronounced gradients in the fields. Eventually the mesh is restructured in such a way that nodes concentrate at areas with high gradients, while the discretization becomes rougher (larger elements) in not so important regions, as the bottom support. Due to the internal rearrangement of the nodes the stress distribution becomes smoother, see Fig. 9c. As in the 2D example the mesh rearrangement results in a softening of the structure. In Fig. 11 the increase of the lowering w of the central point of the block is reported. This lowering increases as the mesh is modified, as the stiffness of the discretization is reduced.

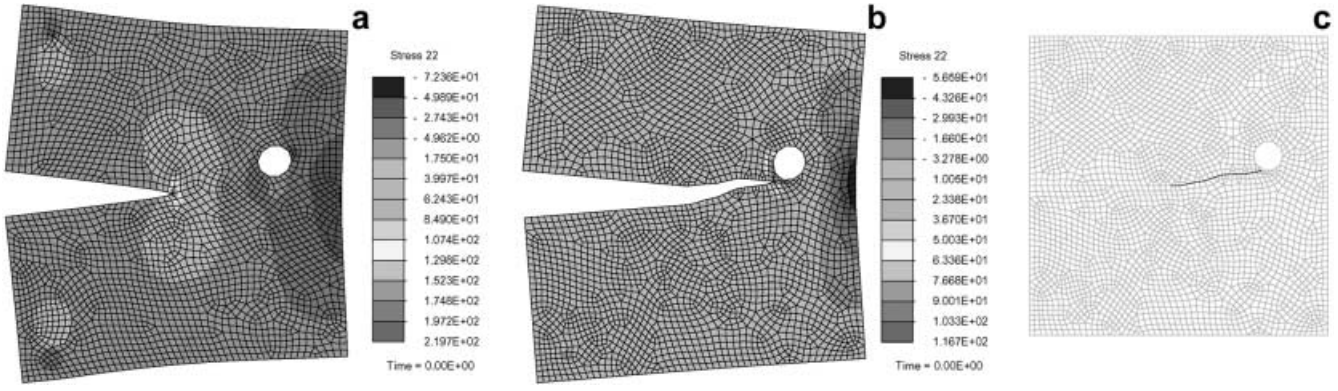

Fig. 7. Crack propagation: **a** initial, **b** finial distribution of σ_{22} in deformed configuration, **c** crack path

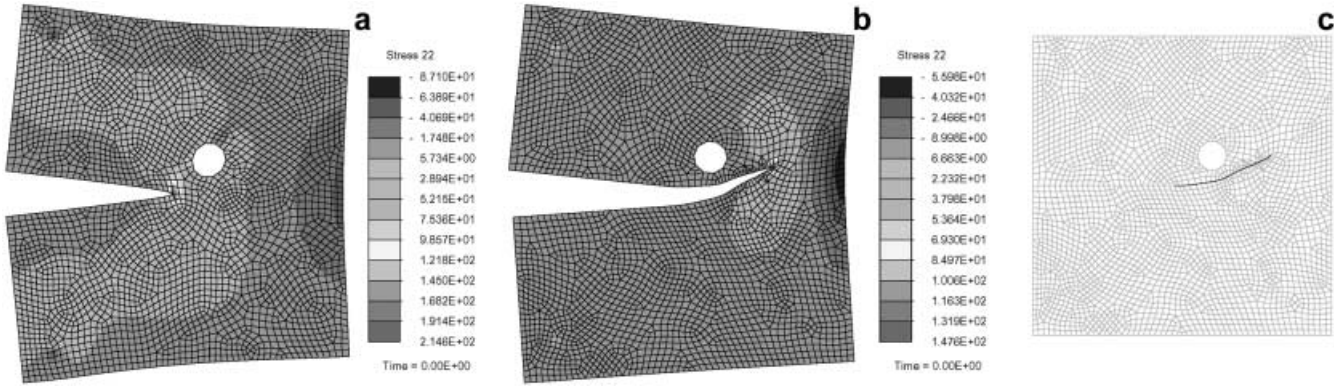

Fig. 8. Crack propagation: **a** initial, **b** finial distribution of σ_{22} in deformed configuration, **c** crack path

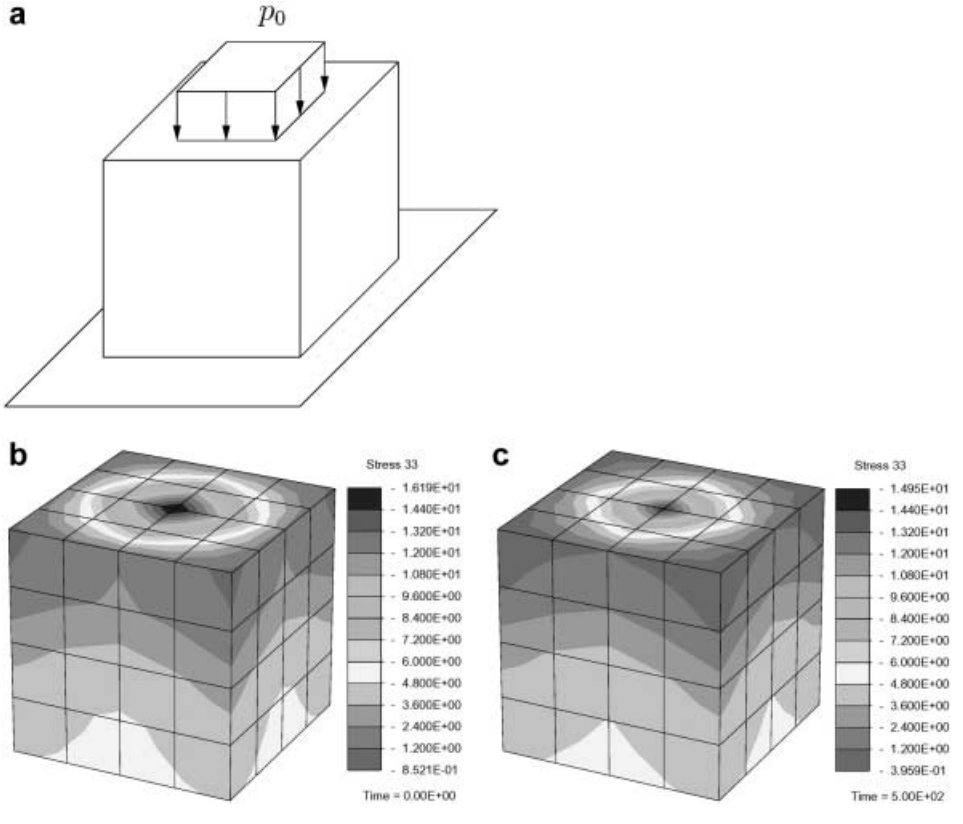

Fig. 9. Block under constant pressure: **a** sketch of the problem, **b** initial distribution of σ_{33}, **c** distribution of σ_{33} after mesh update

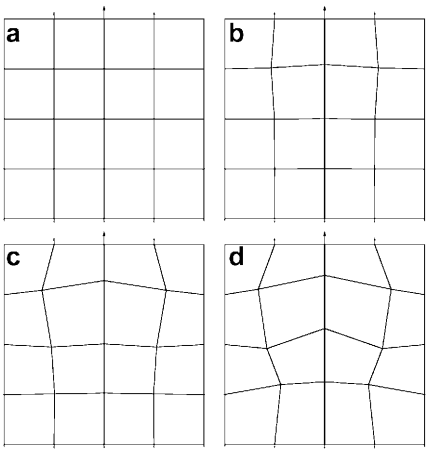

Fig. 10. Cut of the block during mesh update: **a** initial mesh, **b** 10 iterations, **c** 50 iterations, **d** 500 iterations

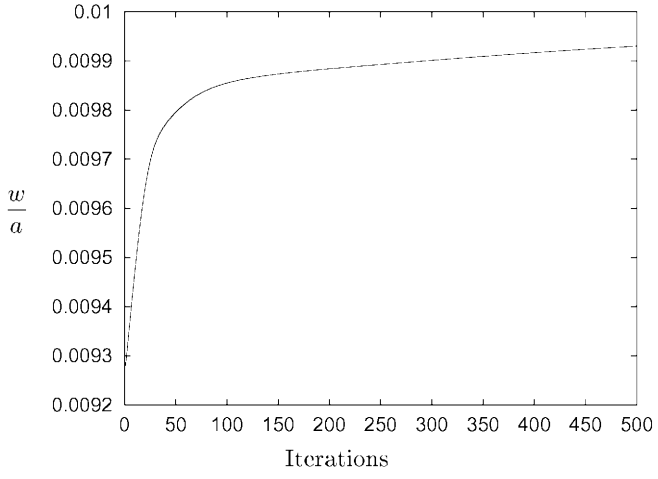

Fig. 11. Change of the vertical lowering w of the central point of the top surface, edge length a

4.6 Material forces at the crack front

It is well known from linear elastic fracture mechanics that at the crack tip material forces are related to energy release rates or J-integrals. As a brief example we present a 3D calculation that resembles a CT-specimen. The specimen is loaded by a vertical displacement on the top surface. The distribution of the stress component σ_{33} in the load direction is shown in Fig. 12a. As expected there is a high stress concentration at the crack tip. At this line also large discrete material forces appear. To visualize them a cut along the ligament is given in Fig. 12b. If material forces are large enough to force the crack front to move, it will move in negative direction of the material forces, thus leading to crack propagation. For the movement of the crack front only the component normal to the crack front is relevant thus resulting in a crack propagation that is more pronounced in the middle than on the free surface. This qualitative behavior is observed experimentally and predicted by damage models of the Gurson type, see e.g. Baaser and Gross (1988).

5 Conclusion

A consistent FE implementation of configurational forces in the context of finite deformation and non-linear elasticity has been presented. Discrete material forces are obtainable by a post-processing step. Once the standard field equations are solved the material forces can be computed in a straightforward way consistent with the discretization. The physical meaning of material forces was discussed concerning changes in the reference configuration (movement of a hole) and concerning fracture mechanics problems. Despite these physical interpretations a computational application was demonstrated. Discrete material forces were used to modify the mesh, i.e. the node positions, in such a way, that the discretized material force balance is satisfied. The examples showed a reduction of the stiffness of the discretizations (FE discretizations are in general stiffer than the exact solution). It was also observed that results for the stresses were smoothed out across element edges.

During all the mesh modifications the topology (connectivity) of the mesh remained unchanged. For future work it seems interesting to investigate the possibility of the use of the material force balance in an adaptive scheme. In a homogeneous body without body forces the

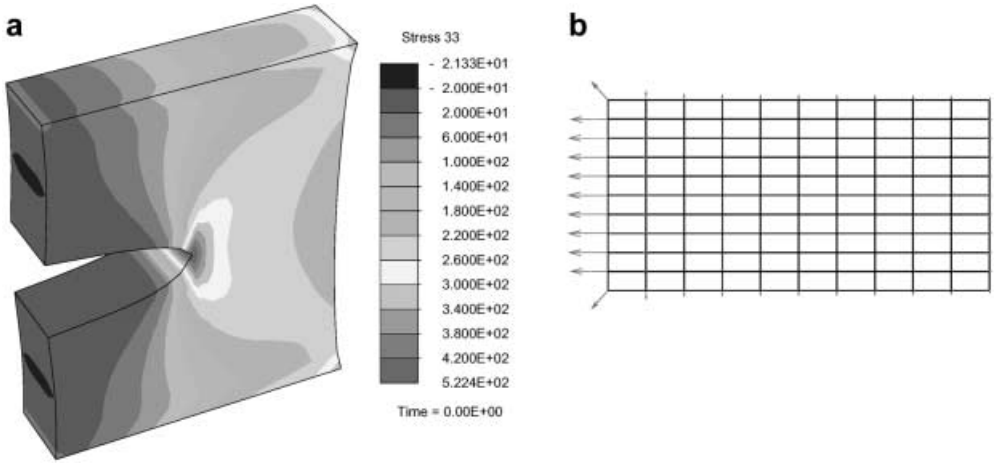

Fig. 12. Cracked Specimen: **a** distribution of σ_{33}, **b** material forces in the ligament

discrete material force **G** could be used as an indicator, where to refine the discretization. An advantage of the material force is that it provides a vectorial information for a directional refinement process. The realization of this idea and the comparison with other error indicators is left for future work.

References

Baaser H, Gross D (1998) 3D-Simulation of Ductile Crack Growth. In: Carpinteri A, Brebbia CA, (eds), Computational Mechanics Publications, Bologna, Italy

Braun M (1997) Configurational forces induced by finite-element discretization. Proc. Estonian Acad. Sci. Phys. Math. 46(1/2): 24–31

Eshelby JD (1951) The force on an elastic singularity. Phil. Trans. Roy. Soc. London A 244: 87–112

Eshelby JD (1970) Energy relations and the energy-momentum tensor in continuum mechanics. In: Kanninen MF (ed) Inelastic Behaviour of Solids, McGraw Hill, New York, pp. 77–115

Gross D (1996) Bruchmechanik. Springer, New York, Berlin, Heidelberg

Gurtin ME (2000) Configurational forces as basic concept of continuum physics. Springer, Berlin, New York, Heidelberg

Kienzler R, Herrmann G (2000) Mechanics in Material Space. Springer, New York, Berlin, Heidelberg

Maugin GA (1993) Material Inhomogeneities in Elasticity. Chapman & Hall, London, Glasgow, New York, Tokyo, Melbourne, Madras

Maugin GA (2000) Geometry of material space: Its consequences in modern computational means. Technische Mechanik 20(2): 95–104

Mueller R, Kolling S, Gross D (2002) On configurational forces in the context of the Finite Element Method. Int. J. Numer. Meth. Eng. 53: 1557–1574

Steinmann P (2000) Application of material forces to hyperelastic fracture mechanics. I. Continuum mechanical setting. Int. J. Solids Struct. 37(48–50): 7371–7391

Steinmann P, Ackermann D, Barth FJ (2001) Application of material forces to hyperelastic fracture mechanics. II. Computational setting. Int. J. Solids Structures 38(32–33): 5509–5526

Wriggers P (2001) Nichtlineare Finite-Element-Methoden. Springer, Berlin, Heidelberg, New York, Barcelona, Hong-Kong, London, Mailand, Paris, Singapur, Tokio